CMI

www.nature.com/cmi

ARTICLE

Ferroptosis promotes T-cell activation-induced neurodegeneration in multiple sclerosis

Jinyuan Luoqian[1,3], Wenyong Yang[1,3], Xulong Ding[1,3], Qing-zhang Tuo[1], Zheng Xiang[1], Zhaoyue Zheng[1], Yu-jie Guo[1], Li Li[1], Pengbo Guan[1], Scott Ayton[2], Biao Dong[1], Huiyuan Zhang[1], Hongbo Hu[1]✉ and Peng Lei[1]✉

While many drugs are effective at reducing the relapse frequency of multiple sclerosis (MS), there is an unmet need for treatments that slow neurodegeneration resulting from secondary disease progression. The mechanism of neurodegeneration in MS has not yet been established. Here, we discovered a potential pathogenetic role of ferroptosis, an iron-dependent regulated cell death mechanism, in MS. We found that critical ferroptosis proteins (acyl-CoA synthetase long-chain family member 4, ACSL4) were altered in an existing genomic database of MS patients, and biochemical features of ferroptosis, including lipid reactive oxygen species (ROS) accumulation and mitochondrial shrinkage, were observed in the experimental autoimmune encephalitis (EAE) mouse model. Targeting ferroptosis with ferroptosis inhibitors or reducing ACSL4 expression improved the behavioral phenotypes of EAE mice, reduced neuroinflammation, and prevented neuronal death. We found that ferroptosis was an early event in EAE, which may promote T-cell activation through T-cell receptor (TCR) signaling in vitro and in vivo. These data indicate that ferroptosis may be a potential target for treating MS.

Keywords: Ferroptosis; Multiple sclerosis; EAE; Neurodegeneration; ACSL4

Cellular & Molecular Immunology (2022) 19:913–924; https://doi.org/10.1038/s41423-022-00883-0

INTRODUCTION

Multiple sclerosis (MS) is an inflammatory demyelinating disease that is characterized by the infiltration of T cells, B cells, and other immune cells into the central nervous system (CNS). Demyelinating lesions are characterized as active (inflammatory throughout the lesion area), chronically active (inflammation limited to the lesion border), or inactive (lacking inflammatory activity), and both active and inactive lesions are found in MS patients [1]. In addition to demyelinating relapsing lesions, MS is also characterized by progressive neurodegeneration (secondary progression), which results in the accumulation of disability over time. To date, treatments for MS reduce the frequency of relapse but do not impact secondary progression [2]. One particular roadblock is the limited understanding of neuronal death mechanisms in MS.

Experimental autoimmune encephalitis (EAE) in rodents [3] is an attractive animal model to examine disease mechanisms because several drugs for MS were developed using this model. This model is characterized by sensitized T-helper 17 (T_h17) cells (mediate the inflammatory response in the CNS), the demyelination of neurons, damage to motor neurons, and pathological recurrence/relapse-remission. A major difference between MS and EAE is that the latter requires an external immunization step to initiate the condition [4], which provides a time window for intervention.

Iron is a cofactor for a variety of enzymes involved in maintaining the health of oligodendrocytes and myelin and may be a crucial component of remyelination [5]. MRI and histological studies suggest that iron levels are dysregulated in MS, and there is accumulation in gray matter and depletion in normal-appearing white matter [6]. Iron was previously reported to be released after the death of oligodendrocytes in patients with acute MS [7], which may promote neuronal iron accumulation and associated neurotoxicity [8, 9]. Mechanistically, iron promotes the expression of the RNA-binding protein PCBP1, which mediates proinflammatory cytokines, including interleukin-2 (IL-2), in T_h cells [10]. Deferoxamine (DFO), which is an iron chelator, was shown to attenuate the development of EAE [11]. However, it is unclear how iron causes toxicity and whether regulating iron can be beneficial for MS patients.

Ferroptosis is an iron-dependent form of regulated cell death characterized by mitochondrial shrinkage, iron accumulation, and excess lipid peroxidation [12, 13]. Several diseases that share pathological iron accumulation, including cancer, stroke, and Alzheimer's disease, have been linked with ferroptosis [13–16]. In the tumor microenvironment, IFN-γ, secreted by $CD8^+$ T cells, downregulates the expression of cystine glutamate exchanger (xCT), promoting tumor ferroptosis [17]; in $CD8^+$ T cells, CD36 mediates the uptake of fatty acids, which promotes lipid

[1]Department of Neurology and Center for Immunology and Hematology, State Key Laboratory of Biotherapy, National Clinical Research Center for Geriatrics, West China Hospital, Sichuan University, Collaborative Innovation Center for Biotherapy, Chengdu, Sichuan, China. [2]Melbourne Dementia Research Centre, Florey Institute of Neuroscience and Mental Health, The University of Melbourne, Parkville, VIC, Australia. [3]These authors contributed equally: Jinyuan Luoqian, Wenyong Yang, Xulong Ding.
✉email: hongbohu@scu.edu.cn; peng.lei@scu.edu.cn

Received: 18 October 2021 Revised: 8 May 2022 Accepted: 9 May 2022
Published online: 8 June 2022

peroxidation and ferroptosis [18]. The ferroptosis inhibitor Fer-1 was shown to prevent the processing and release of IL-33, promoting the infiltration of inflammatory macrophages into the CNS in acute kidney injury [19]. These findings raise suggest the involvement of ferroptosis in autoimmune diseases such as MS.

Here, we investigated whether ferroptotic signaling was present in MS pathogenesis by comparing human data and using EAE mice. By genetically and pharmacologically modifying ferroptosis, we aimed to elucidate the regulatory mechanism of ferroptosis-mediated T-cell activation in the development of neuroinflammation. By understanding the role of ferroptosis in MS, strategies may be developed to limit demyelination and neuronal death during MS.

MATERIALS AND METHODS

RNA-seq analysis

The expression profiles of MS patients were downloaded from the Gene Expression Omnibus (GEO) database (accession codes: GSE108000 and GSE38010 [20, 21].), and differential expression was assessed with a linear model and the Bioconductor limma package in R (version 3.5.2).

Heatmap preparation

Heatmaps were generated with the Pheatmap package in R (version 3.5.2) (R Foundation), and the z scores were calculated for each gene row using the mean expression of biological replicates.

sgRNA selection

The sgRNAs were designed by online tools (http://crispr.mit.edu/ and https://crispr.cos.uni-heidelberg.de/), and off-target effects were assayed by http://asia.ensembl.org/. The sgRNA sequences with fewer off-target sites were selected for further analysis (target sequences of the sgRNAs used in this study are shown in Table S1). sgRNAs for murine ACSL4 knockdown (KD) were inserted into BbsI-cleaved pssAAV-EF-gRNA to generate the pssAAV-m-ACSL4-sp.g plasmid. Then, the plasmid was cotransfected with pssAAV-EF-cas9 into B16 cells using Lipofectamine 2000 (Life Technologies), and genomic DNA was extracted to examine targeting efficiency using PCR sequencing and T7E1 digestion (the PCR primers used are listed in Table S2).

Adeno-associated viral vector construction and preparation

To knockdown murine ACSL4 with a recombinant adeno-associated virus (rAAV) in vivo, the plasmid pssAAV-mACSL4-sp.g3 was used to produce mACSL4-sp.g3-rAAV8 to knockdown *Acsl4*, and the AAV8-empty vector was used as a control. All rAAV8 vectors were generated by a triple-plasmid cotransfection method in human embryonic kidney 293 cells. The rAAV8 vectors were collected 72 h posttransfection and purified by two rounds of CsCl gradient ultracentrifugation, followed by silver staining and genome copy titration. The viral vectors were aliquoted and stored at −80 °C before use [22].

AAV injection

For intramuscular (IM) injection, 25 μL of the virus with a total titer of 8×10^{12} genome copies was injected into each of the caudal thigh muscles. For stereotaxic injection, the mice were anesthetized with an intraperitoneal injection of pentobarbital (100 mg/kg, P11011, Bioreagent) and fixed on a stereotaxic plate (RWD, Shenzhen, China). The hole was drilled in the bone by a hand drill (RWD, Shenzhen, China). Two microliters of the virus with total titers of 1.5×10^{13} and 2.0×10^{13} was slowly injected into the left cortex (AP = 0.02 mm, ML = −3 mm, DV = 3 mm) and the right cortex (AP = 0.02 mm, ML = 3 mm, DV = 3 mm) relative to the bregma (RWD, Shenzhen, China). The needle was kept in place for an additional 5 min. After injection, the needle was withdrawn, and the wound was sutured.

Animals

Female C57BL/6 mice were used in this study. All mice were purchased from Beijing HFK Bioscience Co., Ltd. and housed in the specific pathogen-free facility at the State Key Laboratory of Biotherapy, (Sichuan University, China). The mice were adaptively fed for 1 week until the experiment began. Animal use and care were approved by the Animal Care Committee of the State Key Laboratory of Biotherapy, Sichuan University according to institutional animal care and use committee guidelines.

EAE induction

Active EAE model in mice. EAE was induced in 7- to 8-week-old female C57BL/6 mice as previously described [23]. Briefly, EAE was induced by subcutaneous immunization in both flanks with an emulsion containing 200 μg of MOG (rat $MOG_{35–55}$; MEVGWYRSPFSRVVHLYRNGK; GLbiochem Ltd.) in 200 μL of PBS (0.01 M, pH 7.4) and an equal volume of complete Freund's adjuvant (CFA, F5881, Sigma-Aldrich) containing 1 mg/mL *Mycobacterium tuberculosis H37RA*. Two hundred nanograms of pertussis toxin (P7208, Merck) per mouse was injected intraperitoneally at 0 and 48 h postimmunization. The mice were scored 10 days after MOG induction.

Adoptive EAE mouse model. The adoptive EAE model was induced as previously described [24]. Briefly, C57BL/6J mice were immunized with 200 μg of $MOG_{35–55}$ in CFA followed by 200 ng of pertussis toxin at 0 and 48 h postimmunization. Draining lymph node cells and spleens were harvested on Day 11, and the cells were cultured for 3 days in the presence of $MOG_{35–55}$ (25 μg/mL) + IL-23 (25 ng/mL, 1887-ML-010/CF, R&D Systems) or $MOG_{35–55}$ (25 μg/mL) + IL-12 (25 ng/mL, 419-ML-010/CF, R&D Systems) + anti-IFN-γ (10 μg/mL, 16-7311-85, Invitrogen) to induce a T_h1 or T_h17 phenotype, respectively. The cells were then stimulated with conditioned medium from ferroptotic neurons induced by RSL3 (10 μM, S8155, Selleck Chemicals) or control medium for 12 h. The cells (3×10^7 cells) were transferred into naïve recipients, and the mice were scored 5 days after the cells were transferred.

Clinical score evaluation. The animals were randomly divided into control or treatment groups. The EAE clinical score was recorded as follows: 0, no clinical disease; 1, tail weakness; 2, hindlimb weakness; 3, complete hindlimb paralysis; 4, hindlimb paralysis and some forelimb weakness; and 5, moribund or dead. The clinical scores were evaluated blindly. The experiments were performed three times independently, and the results from one experiment are shown. All animals with EAE phenotypes (score ≥ 3) were included in the study and are shown in Figs. 1E, 5A, Figs. S7D, G, S9A. For the rest of the EAE experiments, no animals were excluded.

Drug treatments

Liproxstatin-1 (10 mg/kg, S7699, Selleck Chemicals) or vehicle (2% DMSO + 40% PEG300 + 2% Tween 80 + ddH_2O) was intraperitoneally administered to C57BL/6 mice 17 days postimmunization for 7 days (repeatedly every other day). Human ceruloplasmin (Cp, H130212, Biofarma, Ukraine) [25] or vehicle (saline) was intraperitoneally administered to C57BL/6 mice 17 days postimmunization for 7 days (repeatedly every other day).

Mouse tissue preparation

The mice were anesthetized with an overdose of pentobarbitone (100 mg/kg, P11011, Bioreagent) and perfused with ice-cold PBS (0.01 M, pH 7.4). The cortex and spinal cord weight were recorded, and the tissue was stored at −80 °C before use.

Western blot analysis

Samples were homogenized in cell lysis buffer (P0013, Beyotime) supplemented with the protease inhibitor phenylmethylsulfonyl fluoride (1:100, ST507, Beyotime) and centrifuged at 12,000 × *g* for 30 min. The supernatant was collected, and the total protein concentration was determined with a BCA protein assay kit (P0011, Beyotime). Equal amounts of protein were separated in 4–12% bis-Tris gels with MOPs running buffer at 140 V for 1.5 h and then transferred to nitrocellulose membranes by a Trans-Blot system at 100 V for 1 h. Then, the membranes were washed with 1 × TBST for 5 min at room temperature (20 °C), shaken, and blocked with 5% skim milk in 1 × TBST for 1 h at room temperature. For immunoblot analysis of protein phosphorylation, naïve $CD4^+$ T cells were isolated from the spleen and LNs of C57BL/6 mice (6–8 weeks old) using magnetic beads (Miltenyi Biotec) and cultured for 1 h with medium harvested from primary neurons treated with the GPX4 inhibitor RSL3 (10 μM, 24 hr) or directly with RSL3 (10 μM). The cells were stimulated with anti-CD3 (1 μg/ml) and anti-CD28 (1 μg/ml) in treated medium for different times and lysed in kinase cell lysis buffer supplemented with phosphatase inhibitors [26, 27] for western blotting. In this study, the following antibodies were diluted in 1 × TBST as indicated: 1:10,000 for anti-ACSL4 (ab155282, Abcam); 1:5000 for anti-GPX4 (ab125066, Abcam); 1:1000 for anti-Akt (9272, Cell Signaling Technology); 1:1000 for anti-phospho-Akt (Ser473) (4060, Cell Signaling Technology); 1:1000 for anti-p44/42 MAPK (Erk1/2) (9102, Cell Signaling Technology); 1:1000 for anti-phospho-p44/42 MAPK (Erk1/2)

(Thr202/Tyr204) (4370, Cell Signaling Technology); 1:10,000 for anti-mouse Ig (A9044, Sigma-Aldrich); 1:10,000 for anti-rabbit Ig (A0545, Sigma-Aldrich); 1:10,000 for anti-GAPDH (G8795, Sigma-Aldrich); 1:10,000 for anti-β-actin (A5441, Sigma-Aldrich). All uncropped images of the western blots are shown in Supplementary Fig. S10.

Lipid peroxide assay

A Lipid Hydroperoxide (LPO) Assay Kit (A106, Nanjing Jiancheng Bioengineering Institute) was used to measure the lipid peroxidase level in brain tissue or spinal cord lysates. Briefly, the tissue samples were homogenized in PBS (0.01 M, pH 7.4) and centrifuged at 12,000 × *g* for 10 min. The supernatant was collected, and the total protein concentration was determined with a BCA protein assay kit (Beyotime). The pellet was used for the lipid peroxide assay. Lipid peroxidation produced a stable chromophore at 45 °C for 60 min, with a maximum absorption peak at 586 nm. The concentration of malondialdehyde (MDA) in mouse tissue was measured using a Lipid Peroxidation MDA Assay Kit (S013M, Beyotime). Briefly, the tissue samples were homogenized in cell lysis buffer (P0013, Beyotime) and centrifuged at 12,000 × *g* for 10 min. The supernatant was collected, and the total protein concentration was determined with a BCA protein assay kit (Beyotime). The pellet was used for the MDA assay. MDA reacts with thiobarbituric acid (TBA) at 100 °C for 15 min, with a maximum absorption peak at 535 nm.

Lipid ROS assay

A single-cell suspension was prepared to quantify lipid peroxidation in animal samples. Spinal cord tissue was removed and cut into small pieces, and then the tissue was mechanically minced with a 70 μM cell strainer and washed with PBS. The spinal cord mixed cells were digested by Collagenase Type IV (0.1–0.3 mg/ml, 17104-019, Thermo Fisher) for 60 min at 37 °C in a water bath and centrifuged at 1500 rpm for 5 min. Lipid peroxidation in cells was assessed as previously described [22]. Briefly, cells were incubated with BODIPY 581/591 C11 (1 μM; Thermo Fisher) for 30 min at 37 °C in a tissue culture incubator stained with BODIPY 581/591 C11. Subsequently, the cells were resuspended in 500 μL of fresh PBS (DPBS, Gibco), strained through a 40 μM cell strainer (BD Falcon), and analyzed using the 488 nm laser on a flow cytometer (LSR Fortessa, BD) for excitation. The signals from both nonoxidized C11 (PE channel) and oxidized C11 (FITC channel) were measured. The ratio of the mean fluorescence intensity (MFI) of FITC to the MFI of PE was calculated for each sample. In other cases, only the signal from oxidized C11 was measured, and the MFI of FITC was calculated. The data were normalized to control samples as shown by the relative lipid reactive oxygen species (ROS) levels. Data analysis was conducted using FlowJo 10.

Inductively coupled plasma–mass spectrometry (ICP–MS)

Tissue samples were freeze-dried by a lyophilizer, dissolved in 65% nitric acid overnight at room temperature, and then boiled at 90 °C for 20 min. An equal volume of 30% H_2O_2 was added to the samples and incubated at 70 °C for 20 min. Ion levels were measured by ICP–MS (7900, Agilent). The results were normalized to the tissue wet weight.

RNA extraction, cDNA synthesis, and quantitative real-time PCR

Total RNA was isolated from tissues by TRIzol reagent (15596026, Thermo Fisher), and cDNA was synthesized using the SuperScript™ IV First-Strand Synthesis System (18091050, Invitrogen). Quantitative PCR was performed using SYBR Green reagent (Bio–Rad). Gene expression was normalized to *GAPDH* using the ΔΔCt method. The results are expressed as the fold change and were normalized to the controls. The primer sequences are listed in Table S3. Naïve $CD4^+$ T cells were isolated from the spleen and lymph nodes (LNs) of C57BL/6 mice (7–8 weeks old) using magnetic beads (130-117-043, Miltenyi Biotec) and were immediately treated with medium harvested from primary neurons treated with the ferroptosis activator RSL3 (10 μM, 24 h) or erastin (5 μM, 24 h), stimulated with plate-bound anti-CD3 (1 μg/ml) and anti-CD28 (1 μg/ml) in the presence of RSL3 or erastin for different times, and then subjected to RNA extraction.

Transmission electron microscopy

The mice were anesthetized with pentobarbitone (100 mg/kg, P11011, Bioreagent) and perfused with ice-cold PBS (0.01 M, pH 7.4). The spinal cord and cortex were removed and dissected into 1 mm^3 sections and then perfused with 2.5% glutaraldehyde for 4 h at 4 °C. The tissues were treated with 1% osmium tetroxide for 2 h at 20 °C, dehydrated in gradient ethanol (50–100%), embedded in epoxy resin, and polymerized for 48 h at 60 °C. The samples were stained with uranyl acetate (80 nm) and lead citrate before transmission electron microscopy analysis (HT7700, HITACHI). Images were captured with a Slow Scan CCD camera and iTEM software (Ver: 01.07, Olympus Soft Imaging Solutions).

Histological analysis

The mice were anesthetized with pentobarbitone and perfused with ice-cold PBS (0.01 M, pH 7.4). The spinal cord and cortex were removed, dissected into 1 mm^3 sections, perfused with 4% paraformaldehyde and postfixed overnight. The paraffin-embedded sections (5 μm) of spinal cord were stained with H&E to visualize inflammatory infiltration, Luxol fast blue (LFB) to evaluate demyelination, or Nissl to assess the number of neurons. The images were analyzed with Pannoramic MIDI and CaseViewer software 2.4 (3DHIESTECH Ltd.).

Immunofluorescence analysis

All tissues (spinal cord and brain) were embedded in paraffin and cut to a thickness of 5 μm. The tissue sections were incubated with 0.1% Triton X-100 (diluted with PBS) after antigen retrieval for 30 min and were blocked with 5% goat serum (diluted with 0.1% Triton X-100) for 1 h. The primary antibodies for immunofluorescence were anti-NeuN (62994, Cell Signaling Technology, 1:100), anti-Myelin Basic Protein (78896, Cell Signaling Technology, 1:100), anti-GFAP (3657, Cell Signaling Technology, 1:100), anti-ACSL4 (ab155282, Abcam, 1:500), and Alexa Fluor-labeled antibodies (Invitrogen, 1:500). Fluorescently-labeled sections were visualized on a confocal laser-scanning microscope (Nikon ECLIPSE Ti-S). Brightness and contrast alterations were applied identically on captured images using CaseViewer software 2.4.

Rotarod treadmill test

The motor coordination of the animals was measured after surgery and treatment using a rotarod treadmill for mice (RWD, Shenzhen, China) in the accelerating rotor mode (10 speeds from 4 to 40 r.p.m. for 5 min). The interval from when the animal mounted the rod to when it fell off was recorded as the retention time, and mice that lasted for 300 s on the accelerating rotating rod were recorded as survivors. The animals were trained for 2 days, 3 trials per day, and the mean duration on the rod was recorded to obtain stable baseline values. Performance on the rotarod test was measured three times per day in 1 week during Lip-1 or Cp treatment.

Flow cytometry

Infiltrating T cells in the CNS were enriched using density gradient centrifugation (Percoll, P1644, Sigma-Aldrich). The cell pellet was stimulated with 1 μL of PMA (50 ng/mL, Sigma-Aldrich), 1 μL of ionomycin (1 μg/mL, Sigma-Aldrich), and 1 μL of monensin (2 μM, Sigma-Aldrich) for 4 h and then stained with the following antibodies: anti-CD45 (APC-Cy7, 561037, BD Biosciences, 30-F11), anti-CD4 (FITC, 553046, BD Biosciences, RM4-5), anti-CD8 (BV510, 563068, BD Biosciences, 53-6.7), anti-IFN-γ (APC, 505809, Biolegend, XMG1.2), and anti-IL-17A (PE, 506904, Biolegend, TC11-18H10.1). The stained cells were analyzed by an LSR Fortessa II (BD Biosciences), and the data were analyzed by FlowJo 10.

Primary neuronal culture and medium collection

Primary cortical neurons were harvested from C57BL/6 mice on embryonic Day 14. The cortices were removed and separated from the meninges, chopped into <1 mm portions in cold KREBS buffer, and dissociated in 0.016% (w/v) trypsin (T2600000, Sigma-Aldrich). The neurons were plated on poly-d-lysine–coated 6-well plates in Dulbecco's modified Eagle's medium (supplemented with 10% fetal bovine serum, 5% horse serum, 50 μg/ml gentamicin (Life Technologies, Inc.)) and incubated overnight (37 °C, 5% CO_2). The plating medium was replaced with neurobasal culture medium (Gibco) supplemented with 2% B27 supplement (Life Technologies), 0.25% GlutaMAX (Life Technologies), and 50 μg/ml gentamicin (Life Technologies). At 3 days in vitro (DIV), cytosine arabinoside (Sigma-Aldrich) was added to the neurons in neurobasal medium to achieve a final concentration of 2 μM (to reduce astrocytic growth). At 4 DIV and 11 DIV, two-thirds of the medium was replaced with fresh neurobasal medium before treatment on 14–15 DIV. The medium was collected 24 h after RSL3

or erastin administration, centrifuged at 1500 × *g* for 10 min in a cold room (4–8 °C), and stored at −80 °C until use.

Statistical analysis

The data are shown as individual values. Statistical analysis was performed using GraphPad Prism 8.0 software, and the data are presented as the mean ± SEM. Statistical methods are indicated in the figure legends. *P* values <0.05 were considered significant.

RESULTS

Ferroptosis activation in the spinal cords of EAE mice

We first examined whether biochemical changes consistent with ferroptosis were present in EAE mice. Iron levels in the spinal cord were elevated in the EAE mouse model (~250%; $p = 0.0044$; Fig. 1A), which was consistent with previous reports [6, 28, 29]. Copper, zinc, and calcium levels were not altered (Fig. S1A–C). Significant increases in malondialdehyde (MDA), lipid ROS (measured by C11-BODIPY$^{581/591}$ staining) (Fig. 1B, C), and lipid hydroperoxide (LPO) (Fig. S1D) accompanied the increase in iron after EAE, which indicated ferroptosis. Mitochondrial shrinkage, which is a morphological feature of ferroptosis, was also observed in the spinal cords of EAE mice (Fig. 1D). Specific iron accumulation was observed in the cortical tissue of EAE mice (Fig. S1E–H), but there were no changes in lipid oxidative stress markers (Fig. S1I, J), which was consistent with the pathology of EAE in the spinal cord.

To exclude the possibility that adjuvant-induced nonspecific inflammation may affect these observations, we compared the model to CFA injection alone without MOG. The injection of CFA without MOG did not induce EAE phenotypes (Fig. S2A) or cause lipid peroxidation as indicated by MDA levels (Fig. S2B).

The ferroptosis inhibitor liproxstatin-1 (Lip-1, 10 mg/kg, repeatedly every other day, 17 days postimmunization for 7 days, i.p.) significantly rescued the EAE phenotypes, as evidenced by reduced clinical scores (Fig. 1E) and improved motor function on the rotarod (Fig. 1F), without affecting overall survival. Lipid ROS accumulation in EAE mice was also restored by Lip-1 treatment (Fig. 1G), which was consistent with target engagement by this radical trapping agent and the prevention of ferroptosis. Histopathological analysis (Luxol fast blue staining and Nissl staining) of the spinal cord revealed that Lip-1 ameliorated demyelination and neuronal death (Fig. 1H–K). H&E staining indicated that Lip-1 reduced the infiltration of inflammatory cells into the CNS (Fig. S3A, B). Consistently, a marked reduction in CD4$^+$ T cells in the CNS of EAE mice treated with Lip-1 for 7 days starting 17 days postimmunization (repeatedly every other day) was observed, but there were no changes in CD8$^+$ T cells, as revealed by flow cytometry (Fig. 1L, M). These data suggest that inhibiting ferroptosis after the onset of EAE can ameliorate neuroinflammation, behavioral deficits, and neurodegeneration.

ACSL4 mediates ferroptosis in EAE mice

To identify key ferroptotic proteins involved in the pathogenesis of EAE, we examined genes that were previously implicated in ferroptosis [13] in the spinal cords of EAE mice. Several key genes, including *Acsl4*, *Gpx4*, *Fsp1*, and *Lpcat3*, were significantly altered in a manner that was consistent with the occurrence of ferroptosis (Fig. 2A). Further validation at the protein level by western blotting confirmed that ACSL4 was significantly increased as early as 10 days postimmunization, at a timepoint at which no clinical symptoms of EAE were yet observed (Fig. 2B). GPX4 and FSP1 expression levels were downregulated only after symptom onset 17 days postimmunization (Fig. S4A, B). By reanalyzing published RNA sequencing data from two small but independent clinical cohorts [20, 21], we observed increases in *Acsl4* levels in the perilesional chronic active areas (Figs. 2C, S4C) of MS patients. We further confirmed that Acsl4 was significantly expressed during the peak stage of EAE in mice (Fig. S4D).

The spinal cord contains several types of cells, including neurons, glial cells, and blood vessel cells [30]. We then investigated the localization of ACSL4 in different cell types using immunofluorescence staining and found that ACSL4 was mainly expressed in NeuN$^+$ neurons rather than oligodendrocytes (MBP) or astrocytes (GFAP) (Fig. S5A, B).

Next, we knocked down *Acsl4* by intramuscularly administrating adeno-associated virus (AAV8)-EF-Cas9 + AAV8-mACSL4-sp.g3 (KD, 8×10^{12} genomes in 20 μl) or AAV8 empty vectors as the control to investigate the effect of this gene on EAE progression (Fig. 2D). EAE was induced 15 days after AAV injection, and immunofluorescence analysis and western blotting confirmed the significant reduction in ACSL4 protein expression in the spinal cord 32 days after AAV injection (Figs. 2E, S6A) but not in cortical tissue or the spleen, which produces T cells (Fig. S6B, C). *Acsl4* knockdown markedly ameliorated EAE severity and improved the clinical scores of EAE mice (Fig. 2F). Consistent with a reduction in ferroptosis, the levels of MDA, lipid ROS, and LPO after EAE were significantly reduced by *Acsl4* knockdown (Figs. 2G, H, S6D). Further analysis indicated that the recruitment of peripheral immune cells to the CNS was limited in AAV8-*Acsl4*-KD mice 32 days post-AAV injection, as evidenced by significantly reduced numbers of CD4$^+$ T cells (Fig. 2I, J), T_h1 cells and T_h17 cells (Fig. S6E, F). These data collectively suggest that *Acsl4* knockdown in the spinal cord limits the activation of ferroptosis, suppresses the priming and differentiation of T cells, and consequently prevents behavioral deficits after EAE induction.

Ferroptosis is an early pathological event in EAE

EAE is an autoimmune disorder that is driven by autoreactive T cells [31]. It was previously reported that CD8$^+$ T-cell activation triggers ferroptosis in ovarian tumors and subcutaneous melanomas [17, 18]; however, consistent with previous reports [32, 33], CD8$^+$ T cells did not significantly accumulate after the induction of EAE (Fig. 3A, B), as evidenced by a lack of change in the percentage of CD8$^+$ T cells in the spinal cord 10 days postimmunization (without any behavioral phenotypes, priming stage) and 17 days postimmunization (behavioral phenotypes evident, peak stage). In contrast, the percentage of CD4$^+$ T cells was significantly elevated 17 days postimmunization (Fig. 3A, B) but was unaltered at 10 days postimmunization. Therefore, CNS-infiltrating T-cell (mainly CD4$^+$ T cells) proliferation and differentiation were associated with the behavioral phenotypes. The percentages of T_h1 (IFN-γ$^+$) and T_h17 (IL-17A$^+$) cells were increased at an early stage (10 days postimmunization, Fig. S7A, B), indicating that MOG immunization triggered an immune response.

Therefore, we hypothesized that ferroptotic stress may be an early lesion that might stimulate inflammation. Consistent with this hypothesis, we found that lipid peroxidation, as indicated by MDA or LPO levels (Fig. 3C), was significantly elevated 10 days postimmunization, which was an earlier timepoint than CD4$^+$ T-cell activation (17 days postimmunization) and behavioral phenotype manifestations (17 days postimmunization). Iron levels in the spinal cord were unaltered at this timepoint (Fig. 3C), but an increase in iron did not occur during ferroptosis.

To determine whether ferroptotic signaling drives T-cell activation, we measured the T-cell response in EAE mice that were pretreated with Lip-1. Pretreatment with Lip-1 (3 days postimmunization, repeatedly every other day, i.p.) significantly delayed the behavioral phenotypes (Fig. S7C). Treatment with a single dose of Lip-1 during the priming stage (10 days postimmunization, i.p.) significantly reduced the clinical score (Fig. 3D) and the percentage of CD4$^+$ T cells (Fig. 3E, F) 17 days postimmunization.

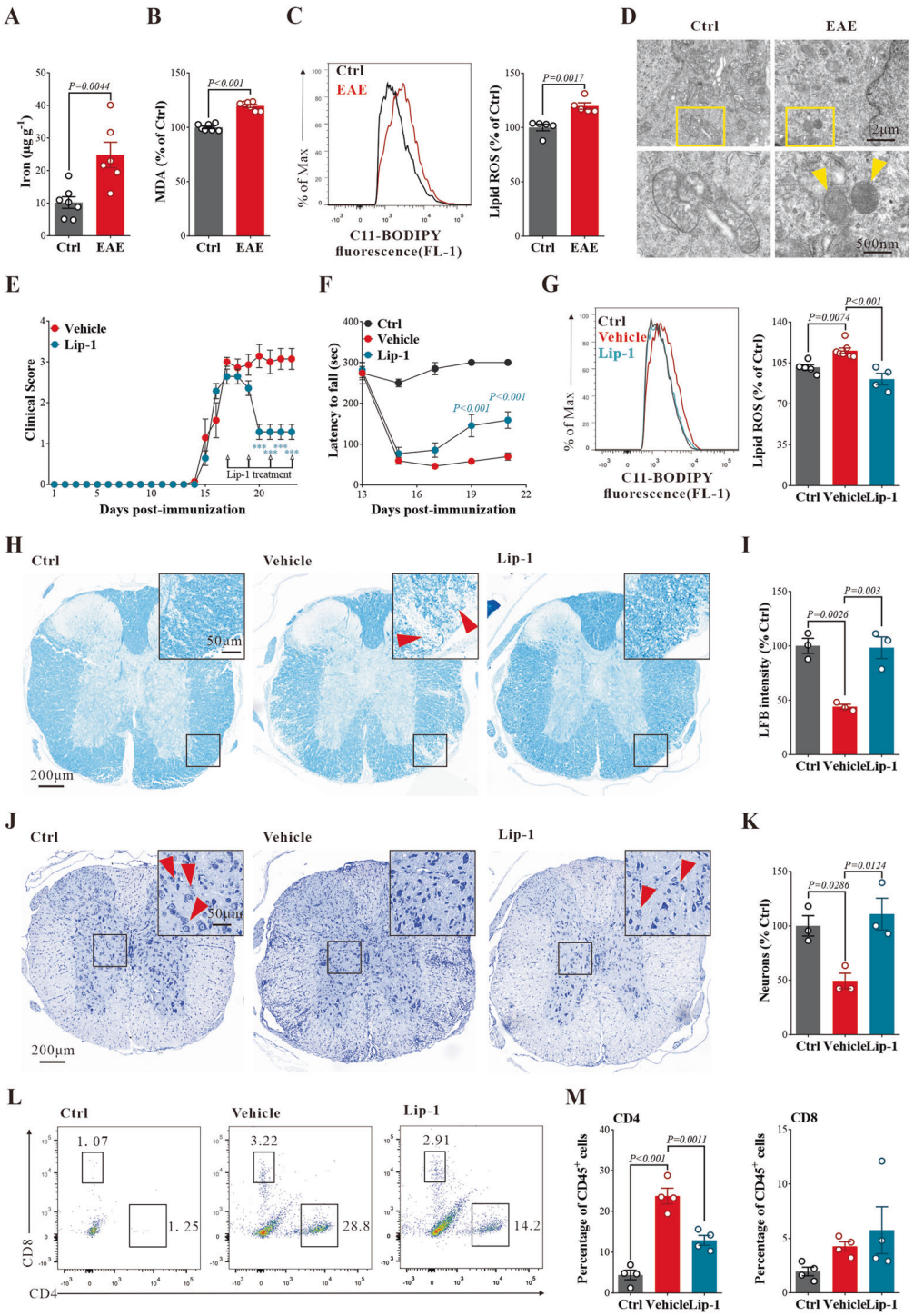

Fig. 1 Ferroptosis in EAE pathogenesis. **A** ICP–MS analyses of the spinal cord tissues of Ctrl and EAE mice on Day 17 postimmunization ($n = 6$). The data were normalized to the tissue wet weight. **B** Lipid peroxidation (MDA) was measured in spinal cord homogenates by MDA assay kits ($n = 7$) and normalized to the protein concentration. **C** Relative lipid ROS levels were quantified by C11-BODIPY$^{581/591}$ (FL-1) in the spinal cord tissues of Ctrl and EAE mice on Day 17 postimmunization ($n = 5$). The data are expressed relative to the Ctrl. **D** Transmission electron microscopy images of neurons in the spinal cords of Ctrl and EAE mice on Day 17 postimmunization. Yellow arrowheads indicate shrunken mitochondria. Scale bars, 2 μm and 500 nm, as indicated. **E** Mean clinical scores after EAE induction, and Lip-1 treatment was started on Day 17 postimmunization ($n = 6$). $^{**}P < 0.01$; $^{***}P < 0.001$. **F** Motor impairments in EAE mice were tested by the rotarod after Lip-1 treatment ($n = 5$). **G** Relative lipid ROS levels were measured by FL-1 in the spinal cords of EAE mice treated with Lip-1. The data are expressed relative to the Ctrl ($n = 4$). **H**–**K** Luxol fast blue (LFB) staining and Nissl staining of spinal cord sections was performed to visualize demyelination and neuronal death, respectively (red arrows) (n = 3). Scale bars, 200 μm and 50 μm, as indicated. **L**, **M** Representative plot and summary graph showing flow cytometric analysis of infiltrating CD4$^+$ and CD8$^+$ T cells in the CNS of EAE mice after Lip-1 treatment ($n = 4$). The data are presented as the means ± SEM. T test (**A**–**C**), two-way ANOVA with Tukey's multiple comparisons test (**E**, **F**), and one-way ANOVA with Tukey's multiple comparisons test (**G**, **I**, **K**, **M**) were used. *P* values are indicated on the graphs

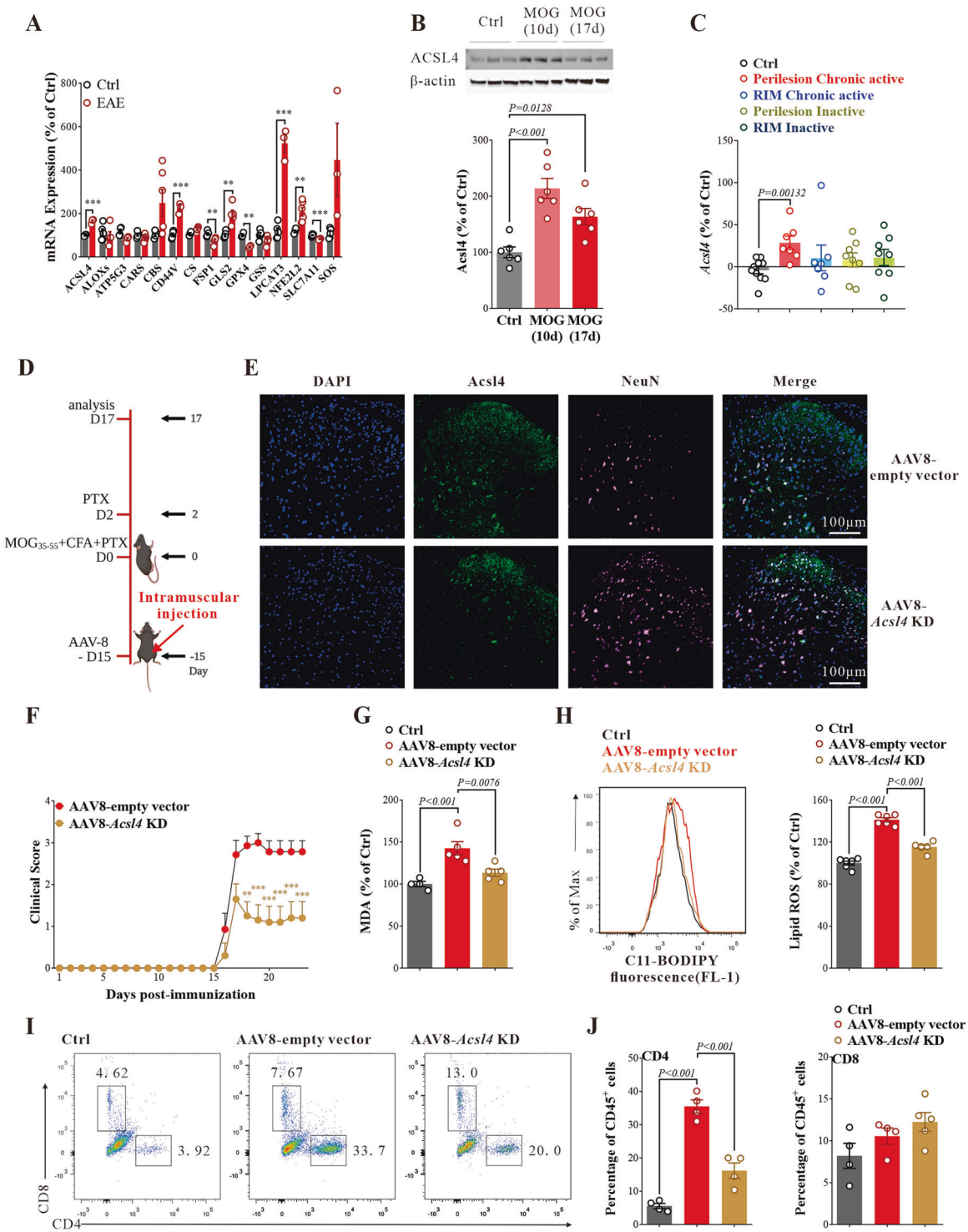

Fig. 2 The role of ACSL4 in mediating neuronal injury caused by ferroptosis. **A** Quantitative PCR (qPCR) analysis revealed elevated expression of ferroptosis-regulating genes in the spinal cord ($n = 3$). $^{**}P < 0.01$; $^{***}P < 0.001$. The data are normalized to *Gapdh* and expressed as the fold change relative to the Ctrl. **B** Western blot analysis of ACSL4 in EAE mice ($n = 6$). The data are normalized to β-actin and expressed relative to the Ctrl. **C** *Acsl4* expression was upregulated in the white matter of MS patients, as measured by microarray analyses ($n = 7$). **D** Diagrammatic drawing of the spinal cord AAV8-*Acsl4*-KD mice. **E** Immunofluorescent colabeling of ACSL4 (green) and neurons (pink). Scale bar, 100 μm, as indicated. **F** Mean clinical scores of AAV8-*Acsl4*-KD mice and control AAV8-empty vector mice ($n = 6$). $^{**}P < 0.01$; $^{***}P < 0.001$. **G** Lipid peroxidation (MDA) in spinal cord homogenates was normalized to protein concentrations ($n = 5$). The data are expressed relative to the Ctrl. **H** Relative lipid ROS levels in the spinal cords of AAV8-*Acsl4*-KD mice and controls on Day 17 postimmunization ($n = 6$). The data are expressed relative to the Ctrl. **I, J** Representative plot and summary graph showing flow cytometric analysis of infiltrating $CD4^+$ and $CD8^+$ T cells in the CNS of AAV8-*Acsl4*-KD mice and controls ($n = 4$). The data are presented as the means ± SEM. T test (**A**), one-way ANOVA with Tukey's multiple comparisons test (**B**, **C**, **G**, **H**, **J**), and two-way ANOVA with Tukey's multiple comparisons test (**F**) were used. *P* values are indicated on the graphs

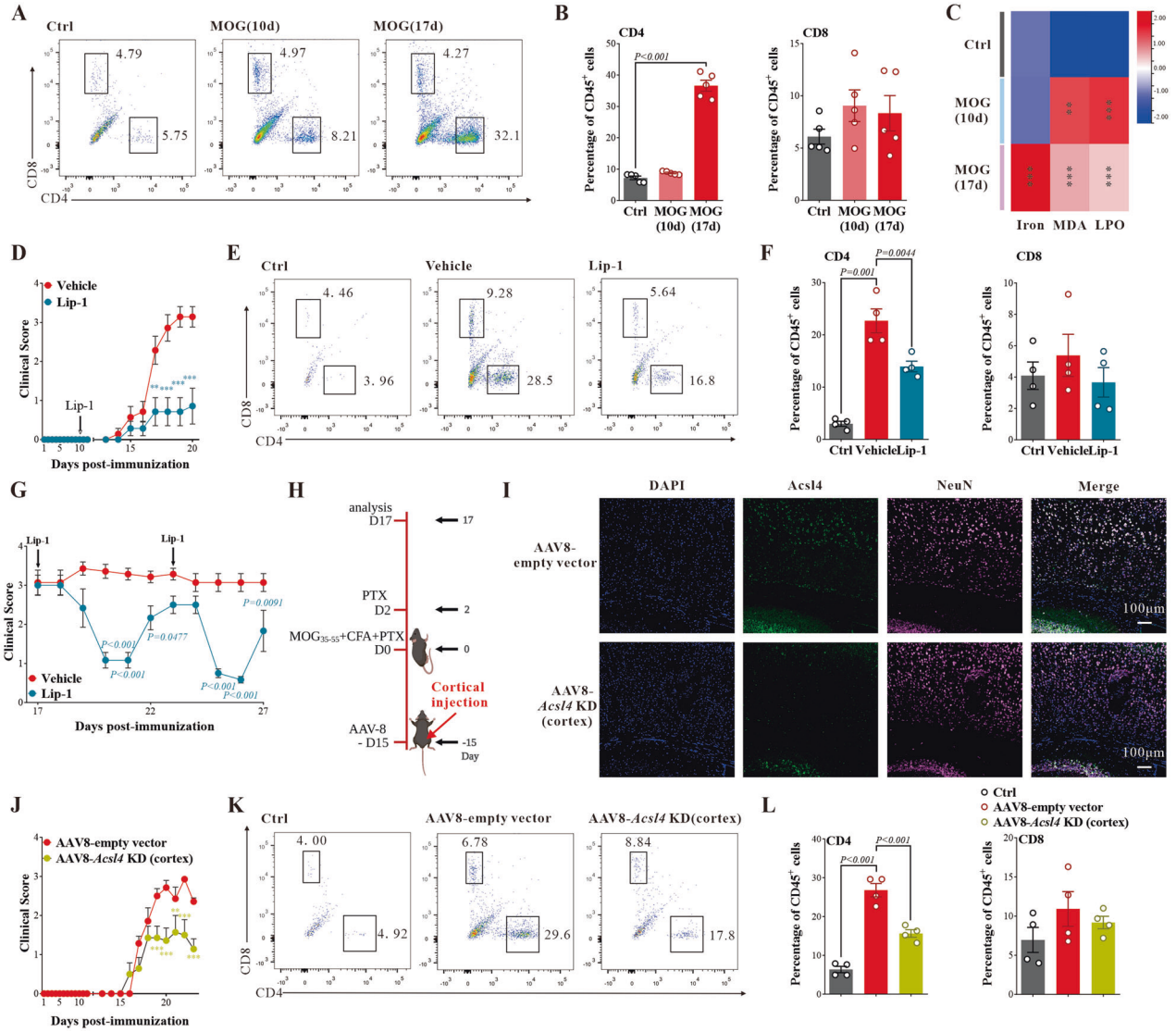

Fig. 3 Ferroptosis is an early event in EAE mice. **A**, **B** Representative plot and summary graph showing flow cytometric analysis of infiltrating $CD4^+$ and $CD8^+$ T cells in the CNS of EAE mice on different immunization days ($n = 5$). **C** The lipid peroxidation (MDA and LPO) and iron levels in the spinal cords of EAE mice ($n = 5$). **D** Mean clinical scores of EAE mice treated with Lip-1 beginning on Day 10 postimmunization ($n = 6$). $^{***}P < 0.001$. **E**, **F** Representative plot and quantified percentages of flow cytometric analysis of immune cells infiltrating the CNS of EAE mice treated with Lip-1 for 7 days beginning on Day 10 postimmunization ($n = 4$). **G** Mean clinical scores of EAE mice treated with Lip-1 on Days 17 and 23 postimmunization ($n = 6$). **H** Diagrammatic drawing of the generation of cortical AAV8-*Acsl4*-KD mice. **I** Immunofluorescent colabeling of ACSL4 (green) and neurons (pink). Scale bar, 100 μm, as indicated. **J** Mean clinical scores of EAE mice with cortical *Acsl4* knockdown ($n = 6$). $^{**}P < 0.01$; $^{***}P < 0.001$. **K**, **L** Representative plot and summary graph showing flow cytometric analysis of infiltrating $CD4^+$ and $CD8^+$ T cells in the CNS of cortical *Acsl4*-knockdown mice and controls ($n = 4$). The data are presented as the means ± SEM. One-way ANOVA with Tukey's multiple comparisons test (**B**, **C**, **F**, **L**) and two-way ANOVA with Tukey's multiple comparisons test (**D**, **G**) were used. *P* values are indicated

We further investigated ferroptotic stress in different stages of EAE by injecting Lip-1 at different times after the onset of EAE. A single dose of Lip-1 administered 17 days postimmunization reduced the EAE behavioral phenotypes; however, this effect only lasted for 2 days (Fig. 3G), after which the motor deficits remerged (Fig. S7D). Injection of a single dose of Lip-1 40 days post-immunization, which is a timepoint at which there was little evidence of activated infiltrating T cells [33, 34] (Fig. S7E, F), did not ameliorate the behavioral phenotypes (Fig. S7G). This finding may indicate that Lip-1 is only effective if the infiltration of T cells has occurred or the mice have developed muscle atrophy in the late stage of EAE [35, 36].

To investigate the importance of the anatomical location of ferroptotic stress, we injected AAV8-EF-Cas9 + AAV8-mACSL4-sp. g3 or empty vectors directly into the cortical regions of mice before inducing EAE. AAV injection reduced the regional expression of ACSL4 in the cortex (Fig. 3H, I) without affecting other tissues, such as the spinal cord (Fig. S7H). However, this reduction in the brain only mildly prevented the onset of EAE, as evidenced by reduced clinical scores (Fig. 3J) and T-cell activation, infiltration and expansion (Fig. 3K, L, Fig. S7I, J), indicating that ferroptosis also occurs in the cerebrum in the late stage of EAE.

Ferroptosis promotes T-cell activation by regulating TCR signaling

Several reports have shown that ferroptosis is involved in T-cell-mediated cytotoxicity and inflammation [10, 17]; however, whether ferroptosis affects T-cell function is unknown. Our data indicated that ferroptosis in neuronal cells might regulate T-cell function in EAE mice. To examine this hypothesis, we cultured

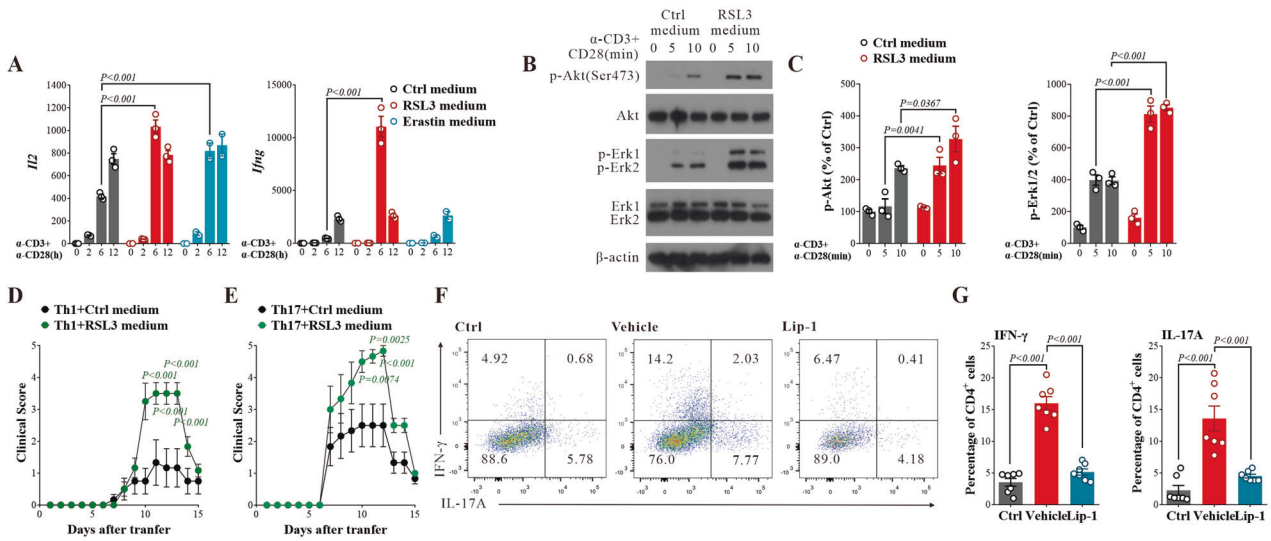

Fig. 4 Ferroptosis promotes T-cell activation. **A** Quantitative PCR analysis of the relative mRNA expression of *Il2* and *Ifng* in T cells treated with or without conditioned medium from cells stimulated with RSL3/Erastin and with anti-CD3 and anti-CD28 antibodies. The data are normalized to *Gapdh* and expressed relative to the Ctrl. **B**, **C** Immunoblot analysis of the indicated phosphorylated (p-) and total proteins in whole-cell lysates if T cells stimulated with anti-CD3 and anti-CD28 antibodies. The data are normalized to the total protein and expressed relative to the Ctrl. **D**, **E** Accelerated manifestations of EAE in T_h1/T_h17 cells cultured with ferroptotic neurons. T_h1/T_h17 cells (3×10^7 cells per mouse) were adoptively transferred into naïve recipients that were monitored for signs of EAE ($n = 6$). **F**, **G** Flow cytometric analysis of T_h1 (IFN-γ^+) and T_h17 (IL-17A$^+$) cells among CD4$^+$ T cells in the CNS of EAE mice treated wit$_h$ Lip-1 ($n = 7$). The data are presented as the means ± SEM. Two-way ANOVA with Tukey's multiple comparisons test (**A**, **C**, **D**, **E**) and one-way ANOVA with Tukey's multiple comparisons test (**G**) were applied. *P* values are indicated

naïve CD4$^+$ T cells with medium harvested from primary neurons treated with the ferroptosis inducer RSL3 (as a GPX4 inhibitor) or erastin (targets xCT) [37] for 24 h. CD4$^+$ T cells were then stimulated with anti-CD3 and anti-CD28, and T-cell activation was measured by cytokine production, as well as T-cell receptor (TCR) proximal signaling events. Quantitative PCR analysis indicated that the supernatant harvested from ferroptotic neurons enhanced the expression of *Il2* and *Ifng* (Fig. 4A), which suggests that ferroptosis promotes T-cell activation. Consistently, immunoblot analysis of TCR proximal signaling events further suggested that ferroptotic stress could facilitate T-cell activation (Fig. 4B, C). This outcome was also evidenced by the activation of several downstream signaling kinases, including Akt and Erk (Fig. 4B, C). When RSL3 was directly cultured with T cells, the TCR signaling pathway was not activated (Fig. S8A, B), indicating that the factors released by ferroptotic neurons may be responsible for T-cell hyperactivation.

We further investigated this hypothesis in vivo using the adoptive transfer EAE model in which T cells from ferroptosis-treated neurons were injected into naive recipients. By transferring pathogenic T_h1 or T_h17 cells (pretreated with conditioned medium from ferroptotic neurons induced with RSL3 or control medium) into recipient mice, we found that culturing T cells with ferroptotic medium significantly exacerbated EAE pathogenesis (Fig. 4D, E), which was consistent with our in vitro findings. We also found that Lip-1 treatment on Day 17 after MOG immunization significantly reduced EAE clinical scores (Fig. 1E). CNS-infiltrating T cells were isolated, and IFN-γ- and IL-17-producing T cells were examined. Compared with T cells from vehicle-treated mice, the T cells isolated from the CNS of Lip-1-treated mice showed reduced IFN-γ and IL-17 production (Fig. 4F, G), indicating impaired T_h1 and T_h17 activation. Collectively, these data indicate that ferroptotic neurons promote T-cell activation, which exacerbates EAE progression.

Targeting ferroptosis with ceruloplasmin to attenuate EAE progression

Ceruloplasmin (Cp) is an extracellular cuproenzyme that oxidizes ferrous iron to ferric iron to promote iron efflux from cells [5] and was previously reported to suppress ferroptosis [38]. Earlier studies indicated the beneficial effects of peripheral Cp treatment in animal models of Parkinson's disease [39] and stroke [40], two diseases in which ferroptosis is implicated [13, 14]. We examined whether peripheral administration of Cp attenuated neuroinflammation in EAE mice. First, we found that Cp (5 mg/kg, injected on Day 17 postimmunization, and repeatedly every other day for 7 days, i.p.) attenuated EAE clinical scores (Fig. S9A). Moreover, Cp treatment 17 days postimmunization dose-dependently ameliorated the clinical deficits of EAE mice (Fig. 5A) and ameliorated motor impairment, as measured by the rotarod (Fig. 5B). Cp treatment also reduced iron levels in the spinal cord (Fig. 5C) and reduced LPO levels (Fig. 5D). Histopathological analysis revealed reduced demyelination and neuronal death in EAE mice treated with Cp (Fig. 5E–H).

We next investigated whether Cp affects T-cell activation in the CNS of EAE mice. H&E staining showed significantly reduced infiltrating inflammatory cells in EAE mice treated with Cp compared to saline-treated mice (Fig. S9B, C). The flow cytometry data indicated a significant reduction in CD4$^+$ T cells in the CNS of mice treated with Cp, but there were no alterations in CD8$^+$ T cells (Fig. 5I, J). Among CNS-infiltrating CD4$^+$ T cells, the percentage of IL-17-producing T cells (T_h17 cells) was greatly reduced by Cp treatment, and a decrease was observed in IFN-γ-producing T_h1 cells (Fig. S9D, E). Collectively, these results demonstrate a potential therapeutic role of Cp in EAE pathogenesis, which may be related to ferroptosis inhibition and/or iron chelation.

DISCUSSION

Here, we demonstrated that ACSL4-mediated ferroptosis induced inflammation and promoted the CNS infiltration and activation of T cells, which may drive neuroinflammation and demyelination in EAE. In neurons, polyunsaturated fatty acids (PUFAs) are esterified by ACSL4 and can be oxidized by iron to generate toxic phospholipid hydroperoxides (PE-AA-OOH) that destroy cellular membranes during ferroptosis. During EAE, ACSL4 and iron levels are increased, resulting in the accumulation of lipid peroxides; this

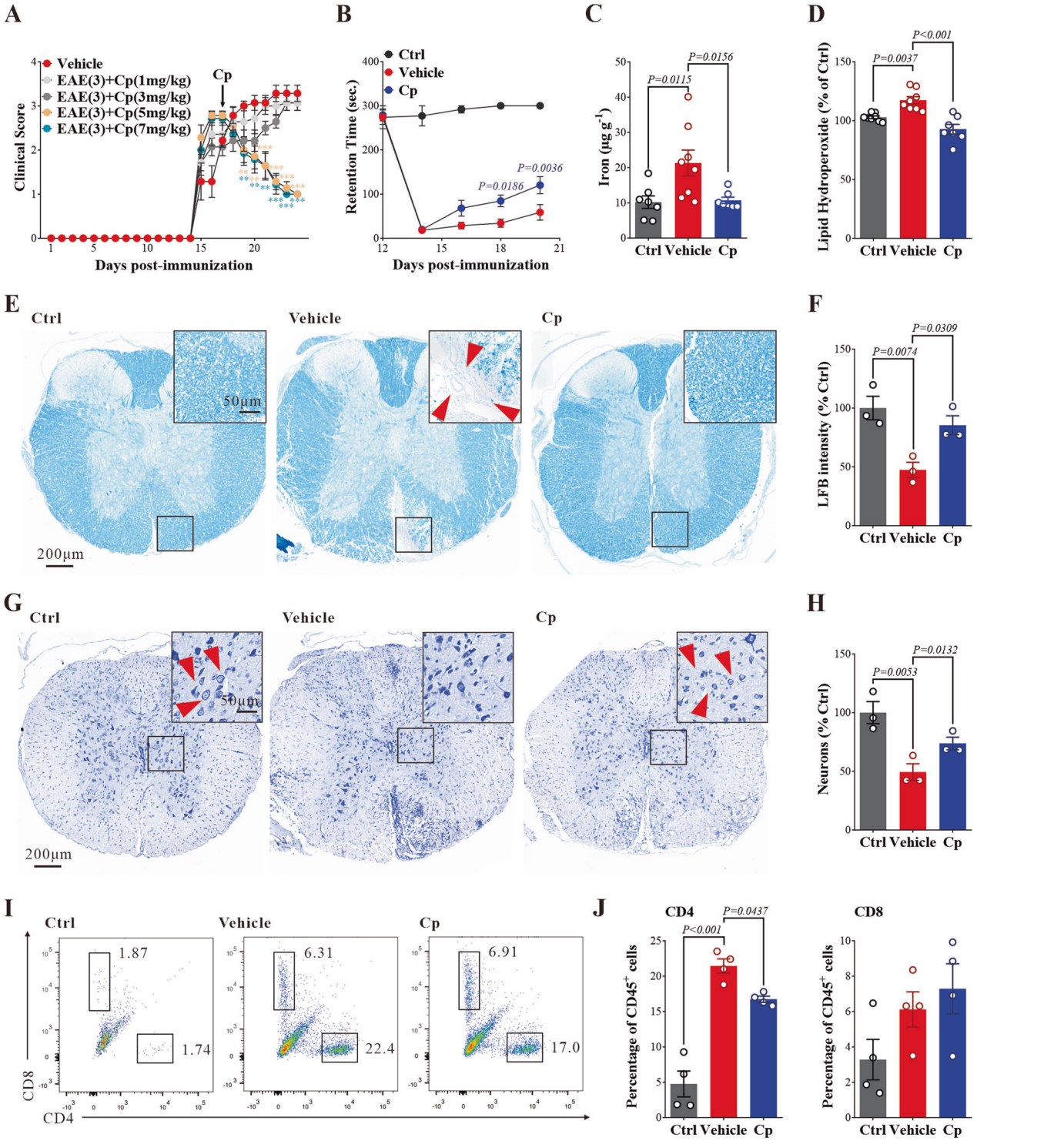

Fig. 5 Cp treatment ameliorates EAE in mice. **A** Mean clinical scores of EAE mice treated with different doses of Cp ($n = 6$). EAE (3) indicates that the treatment was initiated when the mice reached a clinical score of 3. $^{**}P < 0.01$; $^{***}P < 0.001$. **B** Motor impairments in EAE mice were ameliorated by Cp treatment ($n = 5$). **C** ICP–MS analyses of the spinal cords of EAE mice treated with Cp ($n = 7$). The data are normalized to the tissue wet weight. **D** Lipid peroxidation (LPO) was measured in spinal cord homogenates by MDA assay kits ($n = 8$) and normalized to the protein concentration. **E–H** LFB staining and Nissl staining of spinal cord sections from EAE mice treated with Cp (red arrows) ($n = 3$). Scale bars, 200 and 50 μm, as indicated. **I, J** Representative plot and summary graph showing flow cytometric analysis of infiltrating $CD4^+$ and $CD8^+$ T cells in the CNS of EAE mice after Cp treatment ($n = 4$). The data are presented as the means ± SEM. Two-way ANOVA with Tukey's multiple comparisons test (**A**, **B**) and one-way ANOVA with Tukey's multiple comparisons test (**C**, **D**, **F**, **H**, **J**) were used. *P* values are indicated

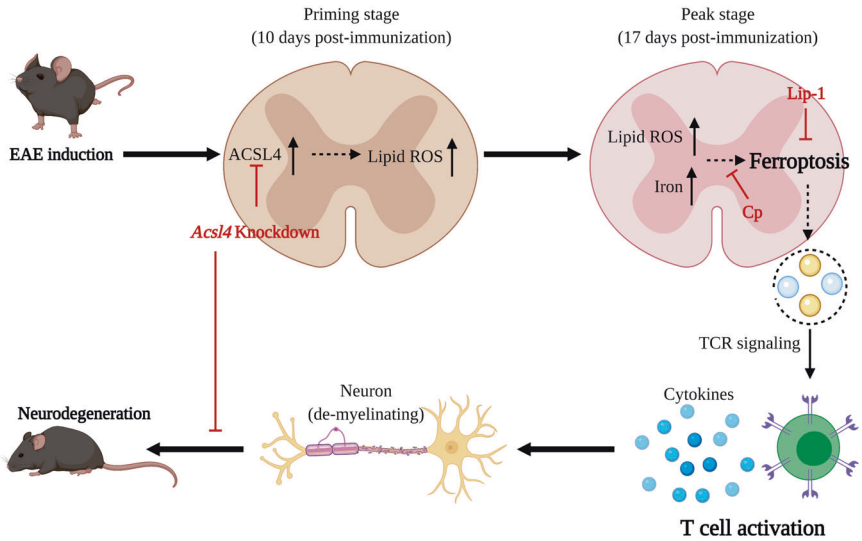

Fig. 6 Working model of ferroptosis in EAE pathogenesis. During EAE development, ACSL4 mediates ferroptosis to induce inflammation and promote the activation of T cells through the TCR signaling pathway, thus driving T-cell-mediated neuroinflammation and demyelination in the spinal cord, which induces EAE pathology. This fiugre was created with BioRender.com.

ferroptotic signaling and the resultant phenotypes were ameliorated by anti-ferroptotic compounds. Ferroptotic neurons secreted factors that promoted T-cell activation and cytokine production in T_h1 and T_h17 cells (Fig. 6).

There have been reports implicating oxidative stress and its regulatory pathways in the pathogenesis of MS. General oxidative damage is present in MS cortical tissues and may be related to oligodendrocyte and neuronal injury [41]. Glutathione (GSH), which is an important antioxidant in ferroptosis [13], was reported to be decreased in EAE [42] and coincided with an increase in oxidative stress. xCT, a control point for the production of glutathione, is elevated during EAE, which may result from the release of glutamate by activated macrophages/microglia [43, 44]. Specific reductions in xCT in immune cells prevents the damage induced by EAE [44]. ACSL4 catalytically promotes the esterification of arachidonic acid (AA), which makes it available for ferroptosis [22], and it was previously reported that IFN-γ plus AA induced ferroptosis in immunogenic tumors via ACSL4 [45]. We showed that ACSL4 was elevated and colocalized with $NeuN^+$ neurons in gray matter, and this increase may result in an increase in PUFAs. Since the mRNA of *Acsl4* was also elevated, we hypothesized that the increase in ACSL4 observed during EAE was transcriptionally regulated, which was previously linked with the transcription factor Sp1 [46] or the transcription coactivator Yes-associated protein (YAP) [47]. Both Sp1 and YAP have been implicated in EAE through their regulation of other proteins [48, 49], and it would be interesting to investigate their links with ACSL4.

We found that during the pathogenesis of EAE, iron accumulation did not occur during the priming stage (Fig. 3C), which was consistent with previous reports [28, 29], but the regulation of ferroptosis and markers of lipid peroxidation were altered. These ferroptotic markers were changed earlier than the proliferation and differentiation of CNS-infiltrating $CD4^+$ T cells, and we demonstrated that ferroptosis promoted T-cell activation. It is known that sufficient free intracellular iron and membrane PUFAs are both prerequisites for ferroptosis [13, 37]. In MS patients, iron was previously reported to be released after the death of oligodendrocytes [7], which may promote neurotoxicity. However, RSL3 inactivates Gpx4, leading to lipid ROS accumulation without affecting iron levels, which can trigger ferroptosis [12]. Similarly, the iron chelator deferoxamine (DFO) inhibits ferroptosis, even when iron has not accumulated [12]. Therefore, iron is required for ferroptosis, and the abundance of iron dictates ferroptotic susceptibility, but an increase in iron does not occur during ferroptosis. In this study, we observed a significant increase in lipid ROS in the spinal cord in an early stage of EAE onset without iron accumulation (Fig. 3C), and this effect was inhibited by Lip-1 (Fig. S7C), indicating that iron accumulation in EAE may be a downstream event that exacerbates ferroptotic stress rather than being the initial trigger of ferroptosis.

We further treated EAE mice with Cp. Cp can transport iron out of neurons [25], prevent ferroptosis [38], and act as a general antioxidant [50]. It was previously reported that Cp-knockout mice developed mild EAE phenotypes at an early stage (13–17 days) and recovered after Day 18 [51]. Another study indicated that Cp was upregulated during the early stage, and iron accumulation was observed during the remission/progressive and late stages [28]. Iron efflux may be impaired during EAE, which causes iron accumulation at a later stage [28]. Mice with complete removal of Cp (knockout mice) are vulnerable to stresses related to iron, such as EAE, and the mice develop MS-like phenotypes [51]. Consistently, we found that adding Cp ameliorated the EAE phenotypes, while iron levels, as well as a specific marker of ferroptosis, were reduced (Fig. 5). Therefore, Cp upregulation may be a mechanism to protect the cells from iron accumulation but is not the cause of iron accumulation, which has been observed in other neuronal disease models, such as Parkinson's disease and ischemic stroke [25, 40].

It has been reported that the ferroptotic checkpoint Gpx4 mediates the removal of phospholipid hydroperoxides that can regulate T-cell immunity [52], and enhanced $CD8^+$ T-cell function results in ferroptosis during cancer immunotherapy [17]. In this study, we found that ferroptosis inhibitors reduced neuroinflammation by regulating T-cell activation in the CNS of EAE mice, providing further evidence that ferroptosis participates in the regulation of immune processes. We found that naïve T-cell activation was enhanced after the cells were cultured with medium harvested from primary neurons treated with ferroptosis inducers. TCR signaling is crucial for the T-cell response and controlling T-cell differentiation [53, 54]. The classic intracellular signals activated by the TCR include mitogen-activated protein kinases (MAPKs, such as the ERK1/2 signaling pathway) [55, 56] and the Akt signaling pathway [57, 58]. The increased TCR signaling in naïve T cells observed in the present study indicates that ferroptotic neurons promote T-cell activation. We further

stimulated T_h1 or T_h17 cells with conditioned medium from ferroptotic neurons induced with RSL3, and after transferring the cells into recipient mice, we found that T cells cultured with ferroptotic medium significantly exacerbated EAE pathogenesis, further supporting our proposed mechanism.

Cell death and immunity are two evolutionarily conserved processes that maintain homeostasis through complex molecular and cellular interactions [59]. Release or exposure of intracellular molecules from dead or dying cells can trigger adaptive immunity, which is beneficial in responding to intracellular pathogens and tumor-associated antigens, but this process may also accelerate the progression of immune diseases such as MS [60]. It was previously reported that the release of danger-associated molecular patterns (DAMPs, such as HMGB1 and ATP) from ferroptotic cancer cells contributed to the maturation of DCs, thereby triggering cytotoxic T-cell-mediated adaptive immunity [61]. Similarly, we propose that ferroptotic neurons regulate the expression of cytokines or chemokines that promote T-cell activation, thus affecting the proliferation and differentiation of T cells.

The function of $CD8^+$ T cells in EAE is not clear. It was previously reported that myelin basic protein (MBP)-specific $CD8^+$ T cells contributed to EAE pathogenesis through the Fas-FasL pathway [62]; $CD8^+$ T cells in EAE can be inhibitory and suppress $CD4^+$ T-cell proliferation [33]. The in vivo data we obtained in the present study suggest that the conditioned medium of ferroptotic neurons enhanced TCR signaling and activation in $CD4^+$ T cells, and it is feasible that $CD8^+$ T cells were also affected by ferroptosis. However, we found that $CD8^+$ T cells were not changed at the time of our analysis (24 days postimmunization), nor did Lip-1 treatment affect $CD8^+$ cells, indicating that $CD8^+$ T cells may not be essential in the priming stage of EAE.

We have demonstrated that ferroptosis inhibition either by small inhibitors, ceruloplasmin protein therapy, or genetic editing prevents early injuries in EAE caused by neuroinflammation. Furthermore, we have provided evidence that preventing ferroptosis may be beneficial for secondary neurodegeneration. Further clinical trials may be warranted to test the efficacy of these compounds, but the development of therapeutic strategies to specifically target ferroptosis-mediated T-cell activation might be useful for inhibiting CNS inflammation and treating MS.

DATA AVAILABILITY

Data supporting this study are available from the corresponding authors upon request.

REFERENCES

1. Kuhlmann T, Ludwin S, Prat A, Antel J, Bruck W, Lassmann H. An updated histological classification system for multiple sclerosis lesions. Acta Neuropathol. 2017;133:13–24. https://doi.org/10.1007/s00401-016-1653-y.
2. Thompson AJ, Baranzini SE, Geurts J, Hemmer B, Ciccarelli O. Multiple sclerosis. Lancet. 2018;391:1622–36. https://doi.org/10.1016/S0140-6736(18)30481-1.
3. Maugh TH 2nd. The EAE model: a tentative connection to multiple sclerosis. Science. 1977;195:969–71. https://doi.org/10.1126/science.195.4282.969.
4. Constantinescu CS, Farooqi N, O'Brien K, Gran B. Experimental autoimmune encephalomyelitis (EAE) as a model for multiple sclerosis (MS). Br J Pharmacol. 2011;164:1079–106. https://doi.org/10.1111/j.1476-5381.2011.01302.x.
5. Hare D, Ayton S, Bush A, Lei P. A delicate balance: Iron metabolism and diseases of the brain. Front Aging Neurosci. 2013;5:34. https://doi.org/10.3389/fnagi.2013.00034.
6. Stephenson E, Nathoo N, Mahjoub Y, Dunn JF, Yong VW. Iron in multiple sclerosis: roles in neurodegeneration and repair. Nat Rev Neurol. 2014;10:459–68. https://doi.org/10.1038/nrneurol.2014.118.
7. Hametner S, Wimmer I, Haider L, Pfeifenbring S, Brück W, Lassmann H. Iron and neurodegeneration in the multiple sclerosis brain. Ann Neurol. 2013;74:848–61. https://doi.org/10.1002/ana.23974.
8. Todorich B, Pasquini JM, Garcia CI, Paez PM, Connor JR. Oligodendrocytes and myelination: the role of iron. Glia. 2009;57:467–78. https://doi.org/10.1002/glia.20784.
9. Kell DB. Iron behaving badly: inappropriate iron chelation as a major contributor to the aetiology of vascular and other progressive inflammatory and degenerative diseases. BMC Med Genom. 2009;2:2. https://doi.org/10.1186/1755-8794-2-2.
10. Wang Z, Yin W, Zhu L, Li J, Yao Y, Chen F, et al. Iron drives T helper cell pathogenicity by promoting RNA-binding protein PCBP1-mediated proinflammatory cytokine production. Immunity. 2018;49:80–92.e7. https://doi.org/10.1016/j.immuni.2018.05.008.
11. Pedchenko TV, LeVine SM. Desferrioxamine suppresses experimental allergic encephalomyelitis induced by MBP in SJL mice. J Neuroimmunol. 1998;84:188–97. https://doi.org/10.1016/s0165-5728(97)00256-7.
12. Dixon SJ, Lemberg KM, Lamprecht MR, Skouta R, Zaitsev EM, Gleason CE, et al. Ferroptosis: an iron-dependent form of nonapoptotic cell death. Cell. 2012;149:1060–72. https://doi.org/10.1016/j.cell.2012.03.042.
13. Yan HF, Zou T, Tuo QZ, Xu S, Li H, Belaidi AA, et al. Ferroptosis: mechanisms and links with diseases. Signal Transduct Target Ther. 2021;6:49. https://doi.org/10.1038/s41392-020-00428-9.
14. Tuo QZ, Zhang ST, Lei P. Mechanisms of neuronal cell death in ischemic stroke and their therapeutic implications. Med Res Rev. 2021;42:259–305. https://doi.org/10.1002/med.21817.
15. Yan HF, Tuo QZ, Yin QZ, Lei P. The pathological role of ferroptosis in ischemia/reperfusion-related injury. Zool Res. 2020;41:220–30. https://doi.org/10.24272/j.issn.2095-8137.2020.042.
16. Lei P, Ayton S, Bush AI. The essential elements of Alzheimer's disease. J Biol Chem. 2021;296:100105. https://doi.org/10.1074/jbc.REV120.008207.
17. Wang W, Green M, Choi JE, Gijon M, Kennedy PD, Johnson JK, et al. CD8(+) T cells regulate tumour ferroptosis during cancer immunotherapy. Nature. 2019;569:270–4. https://doi.org/10.1038/s41586-019-1170-y.
18. Ma X, Xiao L, Liu L, Ye L, Su P, Bi E, et al. CD36-mediated ferroptosis dampens intratumoral CD8(+) T cell effector function and impairs their antitumor ability. Cell Metab. 2021;33:1001–12.e5. https://doi.org/10.1016/j.cmet.2021.02.015.
19. Martin-Sanchez D, Ruiz-Andres O, Poveda J, Carrasco S, Cannata-Ortiz P, Sanchez-Nino MD, et al. Ferroptosis, but not necroptosis, is important in nephrotoxic folic acid-induced AKI. J Am Soc Nephrol. 2017;28:218–29. https://doi.org/10.1681/ASN.2015121376.
20. Hendrickx D, van Scheppingen J, van der Poel M, Bossers K, Schuurman KG, van Eden CG, et al. Gene expression profiling of multiple sclerosis pathology identifies early patterns of demyelination surrounding chronic active lesions. Front Immunol. 2017;8:1810. https://doi.org/10.3389/fimmu.2017.01810.
21. Han MH, Lundgren DH, Jaiswal S, Chao M, Graham KL, Garris CS, et al. Janus-like opposing roles of CD47 in autoimmune brain inflammation in humans and mice. J Exp Med. 2012;209:1325–34. https://doi.org/10.1084/jem.20101974.
22. Tuo QZ, Liu Y, Xiang Z, Yan HF, Zou T, Shu Y, et al. Thrombin induces ACSL4-dependent ferroptosis during cerebral ischemia/reperfusion. Signal Transduct Target Ther. 2022;7:59. https://doi.org/10.1038/s41392-022-00917-z.
23. Grant JL, Ghosn EE, Axtell RC, Herges K, Kuipers HF, Woodling NS, et al. Reversal of paralysis and reduced inflammation from peripheral administration of beta-amyloid in TH1 and TH17 versions of experimental autoimmune encephalomyelitis. Sci Transl Med. 2012;4:145ra105. https://doi.org/10.1126/scitranslmed.3004145.
24. Stromnes IM, Cerretti LM, Liggitt D, Harris RA, Goverman JM. Differential regulation of central nervous system autoimmunity by T(H)1 and T(H)17 cells. Nat Med. 2008;14:337–42. https://doi.org/10.1038/nm1715.
25. Ayton S, Lei P, Duce JA, Wong BX, Sedjahtera A, Adlard PA, et al. Ceruloplasmin dysfunction and therapeutic potential for Parkinson disease. Ann Neurol. 2013;73:554–9. https://doi.org/10.1002/ana.23817.
26. Reiley WW, Jin W, Lee AJ, Wright A, Wu X, Tewalt EF, et al. Deubiquitinating enzyme CYLD negatively regulates the ubiquitin-dependent kinase Tak1 and prevents abnormal T cell responses. J Exp Med. 2007;204:1475–85. https://doi.org/10.1084/jem.20062694.
27. Zhou R, Leng T, Yang T, Chen F, Hu W, Xiong ZG. β-Estradiol protects against acidosis-mediated and ischemic neuronal injury by promoting ASIC1a (Acid-Sensing Ion Channel 1a) protein degradation. Stroke. 2019;50:2902–11. https://doi.org/10.1161/STROKEAHA.119.025940.
28. Zarruk JG, Berard JL, Passos dos Santos R, Kroner A, Lee J, Arosio P, et al. Expression of iron homeostasis proteins in the spinal cord in experimental autoimmune encephalomyelitis and their implications for iron accumulation. Neurobiol Dis. 2015;81:93–107. https://doi.org/10.1016/j.nbd.2015.02.001.
29. Lee NJ, Ha SK, Sati P, Absinta M, Nair G, Luciano NJ, et al. Potential role of iron in repair of inflammatory demyelinating lesions. J Clin Investig. 2019;129:4365–76. https://doi.org/10.1172/JCI126809.
30. Russ DE, Cross RBP, Li L, Koch SC, Matson KJE, Yadav A, et al. A harmonized atlas of mouse spinal cord cell types and their spatial organization. Nat Commun. 2021;12:5722. https://doi.org/10.1038/s41467-021-25125-1.
31. Berard JL, Wolak K, Fournier S, David S. Characterization of relapsing-remitting and chronic forms of experimental autoimmune encephalomyelitis in C57BL/6 mice. Glia. 2010;58:434–45. https://doi.org/10.1002/glia.20935.

32. Caravagna C, Jaouën A, Desplat-Jégo S, Fenrich KK, Bergot E, Luche H, et al. Diversity of innate immune cell subsets across spatial and temporal scales in an EAE mouse model. Sci Rep. 2018;8:5146. https://doi.org/10.1038/s41598-018-22872-y.
33. Saligrama N, Zhao F, Sikora MJ, Serratelli WS, Fernandes RA, Louis DM, et al. Opposing T cell responses in experimental autoimmune encephalomyelitis. Nature. 2019;572:481–7. https://doi.org/10.1038/s41586-019-1467-x.
34. Xiao Y, Jin J, Chang M, Chang JH, Hu H, Zhou X, et al. Peli1 promotes microglia-mediated CNS inflammation by regulating Traf3 degradation. Nat Med. 2013;19:595–602. https://doi.org/10.1038/nm.3111.
35. Pena-Toledo MA, Luque E, Ruz-Caracuel I, Aguera E, Jimena I, Pena-Amaro J, et al. Transcranial magnetic stimulation improves muscle involvement in experimental autoimmune encephalomyelitis. Int J Mol Sci. 2021;22:8589. https://doi.org/10.3390/ijms22168589.
36. Bannerman PG, Hahn A, Ramirez S, Morley M, Bonnemann C, Yu S, et al. Motor neuron pathology in experimental autoimmune encephalomyelitis: studies in THY1-YFP transgenic mice. Brain. 2005;128:1877–86. https://doi.org/10.1093/brain/awh550.
37. Stockwell BR, Friedmann Angeli JP, Bayir H, Bush AI, Conrad M, Dixon SJ, et al. Ferroptosis: a regulated cell death nexus linking metabolism, redox biology, and disease. Cell. 2017;171:273–85. https://doi.org/10.1016/j.cell.2017.09.021.
38. Shang Y, Luo M, Yao F, Wang S, Yuan Z, Yang Y. Ceruloplasmin suppresses ferroptosis by regulating iron homeostasis in hepatocellular carcinoma cells. Cell Signal. 2020;72:109633. https://doi.org/10.1016/j.cellsig.2020.109633.
39. Ayton S, Lei P, Adlard PA, Volitakis I, Cherny RA, Bush AI, et al. Iron accumulation confers neurotoxicity to a vulnerable population of nigral neurons: implications for Parkinson's disease. Mol Neurodegener. 2014;9:27. https://doi.org/10.1186/1750-1326-9-27.
40. Tuo Q, Lei P, Jackman KA, Li X, Xiong H, Li X, et al. Tau-mediated iron export prevents ferroptotic damage after ischemic stroke. Mol Psychiatry. 2017;22:1520–30. https://doi.org/10.1038/mp.2017.171.
41. Fischer MT, Wimmer I, Hoftberger R, Gerlach S, Haider L, Zrzavy T, et al. Disease-specific molecular events in cortical multiple sclerosis lesions. Brain. 2013;136:1799–815. https://doi.org/10.1093/brain/awt110.
42. Morales Pantoja IE, Hu CL, Perrone-Bizzozero NI, Zheng J, Bizzozero OA. Nrf2-dysregulation correlates with reduced synthesis and low glutathione levels in experimental autoimmune encephalomyelitis. J Neurochem. 2016;139:640–50. https://doi.org/10.1111/jnc.13837.
43. Pampliega O, Domercq M, Soria FN, Villoslada P, Rodríguez-Antigüedad A, Matute C. Increased expression of cystine/glutamate antiporter in multiple sclerosis. J Neuroinflammation. 2011;8:63. https://doi.org/10.1186/1742-2094-8-63.
44. Merckx E, Albertini G, Paterka M, Jensen C, Albrecht P, Dietrich M, et al. Absence of system xc(-) on immune cells invading the central nervous system alleviates experimental autoimmune encephalitis. J Neuroinflamm. 2017;14:9. https://doi.org/10.1186/s12974-016-0787-0.
45. Liao P, Wang W, Wang W, Kryczek I, Li X, Bian Y, et al. CD8(+) T cells and fatty acids orchestrate tumor ferroptosis and immunity via ACSL4. Cancer Cell. 2022;40:365–78.e6. https://doi.org/10.1016/j.ccell.2022.02.003.
46. Li Y, Feng D, Wang Z, Zhao Y, Sun R, Tian D, et al. Ischemia-induced ACSL4 activation contributes to ferroptosis-mediated tissue injury in intestinal ischemia/reperfusion. Cell Death Differ. 2019;26:2284–99. https://doi.org/10.1038/s41418-019-0299-4.
47. He S, Li R, Peng Y, Wang Z, Huang J, Meng H, et al. ACSL4 contributes to ferroptosis-mediated rhabdomyolysis in exertional heat stroke. J Cachexia Sarcopenia Muscle. 2022;7:40. https://doi.org/10.1002/jcsm.12953.
48. Huang D, Han Y, Rani MR, Glabinski A, Trebst C, Sørensen T, et al. Chemokines and chemokine receptors in inflammation of the nervous system: manifold roles and exquisite regulation. Immunol Rev. 2000;177:52–67. https://doi.org/10.1034/j.1600-065x.2000.17709.x.
49. Zhang J, Xu X, Liu H, Jin L, Shen X, Xie C, et al. Astrocytic YAP prevents the demyelination through promoting expression of cholesterol synthesis genes in experimental autoimmune encephalomyelitis. Cell Death Dis. 2021;12:907. https://doi.org/10.1038/s41419-021-04203-8.
50. Sideris DP, Petrakis N, Katrakili N, Mikropoulou D, Gallo A, Ciofi-Baffoni S, et al. Ceruloplasmin regulates iron levels in the CNS and prevents free radical injury. J Neurosci. 2002;22:6578–86.
51. Gresle MM, Schulz K, Jonas A, Perreau VM, Cipriani T, Baxter AG, et al. Ceruloplasmin gene-deficient mice with experimental autoimmune encephalomyelitis show attenuated early disease evolution. J Neurosci Res. 2014;92:732–42. https://doi.org/10.1002/jnr.23349.
52. Matsushita M, Freigang S, Schneider C, Conrad M, Bornkamm GW, Kopf M. T cell lipid peroxidation induces ferroptosis and prevents immunity to infection. J Exp Med. 2015;212:555–68. https://doi.org/10.1084/jem.20140857.
53. Hu H, Wang H, Xiao Y, Jin J, Chang JH, Zou Q, et al. Otud7b facilitates T cell activation and inflammatory responses by regulating Zap70 ubiquitination. J Exp Med. 2016;213:399–414. https://doi.org/10.1084/jem.20151426.
54. Snook JP, Kim C, Williams MA. TCR signal strength controls the differentiation of CD4(+) effector and memory T cells. Sci Immunol. 2018;3. https://doi.org/10.1126/sciimmunol.aas9103.
55. Gonzalez-Navajas JM, Fine S, Law J, Datta SK, Nguyen KP, Yu M, et al. TLR4 signaling in effector CD4+ T cells regulates TCR activation and experimental colitis in mice. J Clin Investig. 2010;120:570–81. https://doi.org/10.1172/JCI40055.
56. Bertin S, Lozano-Ruiz B, Bachiller V, Garcia-Martinez I, Herdman S, Zapater P, et al. Dual-specificity phosphatase 6 regulates CD4+ T-cell functions and restrains spontaneous colitis in IL-10-deficient mice. Mucosal Immunol. 2015;8:505–15. https://doi.org/10.1038/mi.2014.84.
57. Klebanoff CA, Crompton JG, Leonardi AJ, Yamamoto TN, Chandran SS, Eil RL, et al. Inhibition of AKT signaling uncouples T cell differentiation from expansion for receptor-engineered adoptive immunotherapy. JCI Insight. 2017;2:348. https://doi.org/10.1172/jci.insight.95103.
58. Wartewig T, Ruland J. PD-1 tumor suppressor signaling in T cell lymphomas. Trends Immunol. 2019;40:403–14. https://doi.org/10.1016/j.it.2019.03.005.
59. Yatim N, Cullen S, Albert ML. Dying cells actively regulate adaptive immune responses. Nat Rev Immunol. 2017;17:262–75. https://doi.org/10.1038/nri.2017.9.
60. Bhat R, Steinman L. Innate and adaptive autoimmunity directed to the central nervous system. Neuron. 2009;64:123–32. https://doi.org/10.1016/j.neuron.2009.09.015.
61. Efimova I, Catanzaro E, Van der Meeren L, Turubanova VD, Hammad H, Mishchenko TA, et al. Vaccination with early ferroptotic cancer cells induces efficient antitumor immunity. J Immunother Cancer. 2020;8:e001369. https://doi.org/10.1136/jitc-2020-001369.
62. Wagner CA, Roque PJ, Mileur TR, Liggitt D, Goverman JM. Myelin-specific CD8+ T cells exacerbate brain inflammation in CNS autoimmunity. J Clin Investig. 2020;130:203–13. https://doi.org/10.1172/JCI132531.

ACKNOWLEDGEMENTS

This work was supported by the National Key Research and Development Project of China (2019YFA0110201), the National Natural Science Foundation of China (82071191, 81801182, 82025002, 32000724, 81871232), and the National Clinical Research Center for Geriatrics, West China Hospital, Sichuan University (2020YJC01, Z2021LC001).

AUTHOR CONTRIBUTIONS

Contribution: PL and HH conceived and raised funds for the study. PL supervised the overall project. JY-LQ performed the in vivo studies with supervision from PL and Q-zT. X-lD, W-yY, LL, and P-bG performed the in vitro studies with supervision from HZ and HH. X-lD analyzed the RNA-seq data with supervision from PL. ZX and Z-yZ prepared the AAV-related experiments with supervision from BD. JY-LQ, PL and HH integrated the data and wrote the drafts of the paper. All authors edited the paper.

COMPETING INTERESTS

The authors declare no competing interests.

ADDITIONAL INFORMATION

Supplementary information The online version contains supplementary material available at https://doi.org/10.1038/s41423-022-00883-0.

Correspondence and requests for materials should be addressed to Hongbo Hu or Peng Lei.